Check for updates

Partially reduced graphene oxide and chitosan nanohybrid membranes for selective retention of divalent cations†

Yangyang Wei, [ID] [a] Jian Wang, [a] Hao Li, [a] Man Zhao, [ID] [a] Huifeng Zhang, [a] Yipeng Guan, [a] Hai Huang, [a] Baoxia Mi [ID] [b] and Yushan Zhang *[a]

A tremendous quantity of brackish water with a high proportion of divalent cations is in great need of water softening. Layer-stacked graphene oxide membranes show potential in membrane processing due to their molecular sieving properties, but show poor selective retention of cations due to unstable interlayer spacing and electrostatic interaction. In this study, a partially reduced graphene oxide (prGO) and chitosan (CS) nanohybrid membrane (prGO–CS) was fabricated to achieve the selective retention of divalent cations by adjusting the configuration and controlling the surface charge. The prGO–CS membrane, which included a CS skin and embedded prGO sheets, showed a performance boost of 98.0% rejection of Mg^{2+} and 95.5% rejection of Ca^{2+} when compared with a CS membrane. The membrane showed good water softening performance for brackish water under low operation pressure with a high Na^+/Mg^{2+} selectivity of 33.8. The excellent performance was attributed to the dense structure and positive charge of prGO–CS.

Introduction

The exploitation of a tremendous amount of brackish water in some typically arid areas, such as northwestern China and southern America, is of particular significance in order to alleviate local water scarcity. However, the divalent cations (Mg^{2+} and Ca^{2+}) in brackish water represent a major hindrance due to their scaling tendencies in practical use. Membrane processing has been applied in brackish water softening, but the selective retention of divalent cations still needs to be improved.

Graphene oxide (GO) shows great potential in membrane processing with attributes such as film-forming properties and molecular sieving.[1,2] The layer-stacked GO membrane has 2D negatively charged nano-channels between adjacent GO sheets, which are employed for the removal of high valence anions due to their physical sieving behaviour and electrostatic repulsion.[3,4] However, the interlayer spacing (d-spacing) of the 2D nano-channels became too large to reject ions due to the swelling effect of the GO membrane in water.[5] The reduction of GO was reported to be an effective strategy to regulate the nano-

channels,[6] although over-reduction may result in low water permeability. In addition, electrostatic attraction between the negatively charged GO and positively charged cations weakens the barrier effect of the "separator" layer for the retention of cations. To overcome these problems, GO-based membranes with a dense structure and desirable charge bearing properties are favoured and achieved via configuration adjustment[7–11] and surface charge controlling.[12,13] Consequently, we present a strategy of building an interaction between GO and positively charged polymers to gain a dense structure and desirable surface charge simultaneously.

Chitosan (CS), a natural polymer with positively charged amino groups, displays excellent reactivity with GO and ease of film-forming.[14,15] CS and GO based membranes were reported to have denser structures than the bare CS membrane and showed an improved performance in ethanol–water separation, proton conductivity and mechanical strength.[16,17] Until now, only a few GO–CS desalination membranes have been reported, which focused on the removal of anions and sodium ions. Gao and coworkers reported a negatively charged composite membrane of O-(carboxymethyl)-CS and GO with a nanoporous structure and high rejection of a divalent anion (Na_2SO_4, 92.9%), but a moderate rejection of a monovalent anion (NaCl, 62.0%).[18] Zou and coworkers developed an additional layer of GO and CS on a commercial reverse osmosis membrane (BW30LE).[19] The salt rejection of NaCl increased from 88.7% to 95.6%. However, the selective retention of cations was still not investigated for a GO and CS hybrid membrane.

[a]The Institute of Seawater Desalination and Multipurpose Utilization, State Oceanic Administration, Tianjin 300192, China. E-mail: yszhang_membr@163.com

[b]Department of Civil and Environmental Engineering, University of California, Berkeley, CA 94720, UK. E-mail: mib@berkeley.edu

† Electronic supplementary information (ESI) available: Solubility of GO and prGO in water, Raman spectra and TGA plots of GO and prGO, XPS spectra, XPS survey spectra and C 1s spectra of membranes, and TGA plots of CS and prGO–CS. See DOI: 10.1039/c8ra01916a

In this work, we propose a facile strategy to tailor partially reduced GO (prGO) and CS hybrid membranes. The partial reduction of GO sheets was undertaken to gain reduced *d*-spacing and decrease negative charges without losing solution processability. A prGO–CS membrane with a CS skin and embedded prGO sheets showed a positive charge and dense structure, which resulted in a high rejection of Mg^{2+} and Ca^{2+} without lowering the water flux. Moreover, the nanohybrid membranes exhibited high Na^+/Mg^{2+} selectivity and demonstrated great promise in brackish water softening under low operating pressures (5 bar or 10 bar).

Experimental

Materials

Natural graphite ($\sim$200 μm), H_2SO_4 ($\geq$98%), $KMnO_4$ ($\geq$99%), aqueous H_2O_2 (30 wt%) and glutaraldehyde (50 wt%) were purchased from Sigma-Aldrich. Chitosan (viscosity > 400 mPa s) was supplied from Aladdin Reagents (Shanghai). Acetic acid, NaCl, $MgCl_2$, $CaCl_2$ and Na_2SO_4 were purchased from Sinopharm Chemical Reagent. Ultrafiltration polysulfone (PS) membranes with an average pore size of 0.1 μm used as supports were purchased from Shenzhen Jiaquan Water Treatment Science & Technology Co. Ltd. Ultrapure water produced from Merckmillipore was used throughout the study.

Synthesis of GO and prGO

A modified Hummers' method was used to prepare the GO aqueous dispersion from natural graphite.[20] 150 mL sulfuric acid was added dropwise to a flask with 5 g natural graphite flakes and the mixture was kept stirring for 0.5 h. Then 15 g $KMnO_4$ was added slowly under vigorous stirring. The mixture was heated to 40 °C, stirred for 6 h, and poured into an ice water bath and allowed to cool to room temperature. Then H_2O_2 (30 wt%) was added dropwise into the mixture until the colour turned bright yellow. GO solution was obtained *via* centrifugation and alternate washing with HCl solution (1 mol L^{-1}) and water. Finally, prGO was obtained *via* the thermochemical reduction of the GO aqueous dispersion at 100 °C for 1 h.

Fabrication of hybrid membranes based on prGO and CS

The CS membrane was fabricated by a blade-coating method. Chitosan (2 wt%) dissolved in an aqueous acetic acid (2 wt%) solution was blade coated on PS membranes and kept flat in dust-free air for 1 day. Then the CS membrane was immersed into NaOH solution (0.2 mol L^{-1}) at 0 °C for 3 h to remove the residual acetic acid. The membrane was then immersed in a mixture of sulfuric acid (1 wt%) and glutaraldehyde (1 wt%) solution for 1.5 h at 60 °C to completely crosslink the CS matrix. The used aqueous NaOH, sulfuric acid and glutaraldehyde could be utilized repeatedly several times to reduce chemical discharge. Finally, the crosslinked CS membrane was thoroughly washed with water. The prGO–CS membrane was prepared by blade coating the prGO–CS composite on the PS membrane followed by the crosslinking process as above. The prGO–CS composite was synthesized *via* the chemical reaction between prGO (0.01 wt%) and CS (2 wt%) under mild stirring at room temperature. The GO and prGO membranes were prepared by the pressure-assisted assembly (2 bar) of GO and prGO solution on the substrate of the PS membrane for comparison of surface charge.[21] All the prepared membranes above were preserved after being dried at 40 °C for 24 h.

Instrumentation

Membrane casting equipment (Elcometer 4340) was used to blade coat the CS casting solution on the PS substrate to prepare the CS membranes. The morphology of the nanosheets (GO and prGO) and the membranes was observed by scanning electron microscopy (SEM, FEI Nova NanoSEM 450) and atomic force microscopy (AFM, AIST-NT SPM Smart SPM™-100). The chemical structures of the nanosheets and the surface chemistry of the membranes were analyzed using attenuated total reflectance-Fourier transform infrared spectroscopy (ATR-FTIR, Thermo Scientific Nicolet iS50). An X-ray diffractometer (XRD, Rigaku MiniFlex 600) in Brag–Brentano geometry (θ and 2θ coupled) was used to confirm the crystalline structures of the nanosheets with a Cu Kα X-ray source ($\lambda = 0.154$ nm) at 40 kV and 15 mA. The samples were scanned from 5° to 15° (2θ) with a step size of 0.02° and a count time of 0.6 s at each point. Thermogravimetric analysis (TGA) was carried out using a thermogravimetric analyser (NETZSCH TG209) under a nitrogen atmosphere from room temperature to 850 °C at a 10 °C min^{-1} heating rate. X-ray photoelectron spectroscopy (XPS) was performed using a K-alpha (Thermo Fisher) system to characterize the elementary composition and chemical bonding configuration of the membranes. All binding energies were referenced to the C 1s neutral carbon peak at 284.8 eV. The surface wettability was characterized on a contact angle goniometer (Shanghai zhongchen JC2000D2). The zeta potential was measured on an electrokinetic analyzer (Anton Paar SurPASS™ 3) based on streaming current measurement. The solute concentration in the permeate and feed solution was evaluated respectively by an electrical conductivity meter for single salt feed solution and inductively coupled plasma mass spectrometry (ICP, Thermo Fisher iCAP Q) for mixed salt feed solution.

Test of membrane performances for the selective retention of divalent cations

The flux and salt rejection were measured by a lab made cross-flow test device. The effective membrane surface area was 19.6 cm^2. Membranes were pressurized at 5 bar for 1 h to achieve a stable water flux. The permeation and rejection were measured using 1 g L^{-1} single salt solution ($MgCl_2$, $CaCl_2$, Na_2SO_4 and NaCl) as feeds at 25 °C. Membrane permeation flux (J, L m^{-1} h^{-1} bar^{-1}), rejection (R, %), Na^+/Mg^{2+} selectivity $\alpha_{Mg^{2+}}^{Na^+}$ and Na^+/Ca^{2+} selectivity $\alpha_{Ca^{2+}}^{Na^+}$ were calculated using eqn (1), (2), (3) and (4) respectively.[22]

$$J = \frac{V}{S \times \Delta t \times \Delta P} \quad (1)$$

$$R = \left(1 - \frac{C_p}{C_r}\right) \times 100\% \quad (2)$$

$$\alpha_{Mg^{2+}}^{Na^+} = \frac{100\% - R_{Na^+}}{100\% - R_{Mg^{2+}}} \tag{3}$$

$$\alpha_{Ca^{2+}}^{Na^+} = \frac{100\% - R_{Na^+}}{100\% - R_{Ca^{2+}}} \tag{4}$$

V is the permeate volume during the measurement time Δt under stable conditions and S is the effective membrane area. ΔP is the *trans*-membrane pressure difference which is simplified into the specified applied pressure. C_p and C_r are the solute concentration in the permeate and feed solution respectively.

Results and discussion

Characterization of GO and prGO nanosheets

The surface topography of GO and prGO nanosheets was characterized by SEM and AFM (Fig. 1). The size distribution of the GO sheets fell into the range of 5 to 30 μm (Fig. 1a) and the thickness was 1.0 nm (Fig. 1c and d) which confirmed the
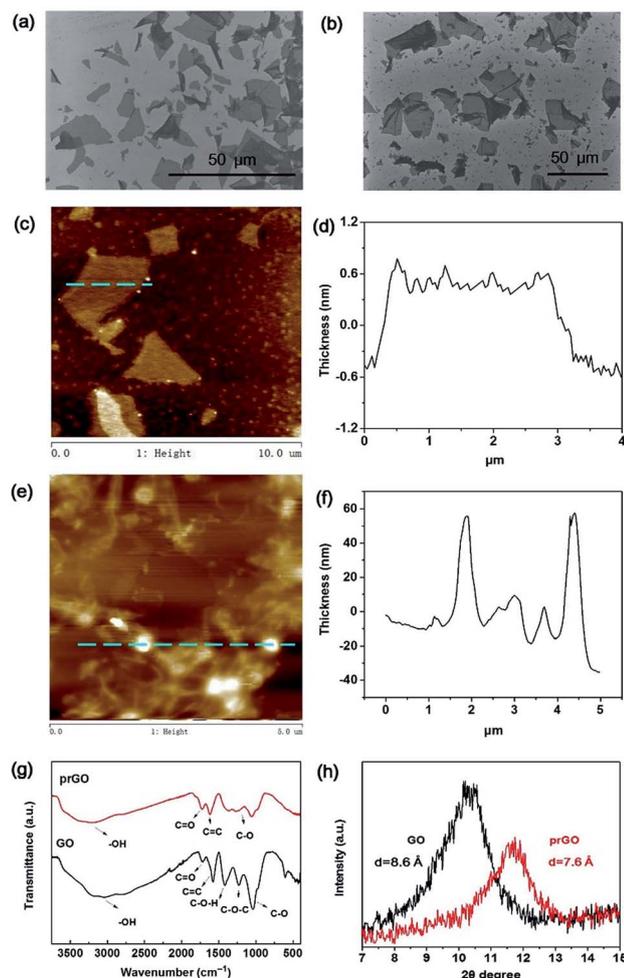

Fig. 1 Morphological and chemical structure analysis of GO and prGO. The SEM images of (a) GO and (b) prGO sheets. The tapping mode AFM topographic images of (c) GO and (e) prGO sheets, and the height profiles of (d) GO and (f) prGO sheets. (g) FTIR-ATR spectra of GO and prGO. (h) XRD spectra of GO and prGO.

successful exfoliation from graphite.[23] In contrast, the prGO sheets presented a more corrugated morphology (Fig. 1b) and were small sheets curled up into nanoparticles with a diameter of 20–60 nm (Fig. 1e and f). This is because the oxygen-containing groups were partially reduced and the electrostatic repulsion in the prGO nanosheets was weakened after thermal treatment.[24] The prGO sheets still showed stable dispersion in water owing to the residual oxygen-containing groups, which provided solution processability in order to fabricate the membranes (Fig. S1†).

The chemical structure and elemental composition of GO and prGO were characterized by FTIR, Raman, XRD and XPS spectroscopy and TGA analysis. The FTIR characteristic peaks of GO (Fig. 1g) were the O–H stretching vibration (3230 cm^{-1}), the C=O stretching vibration (1725 cm^{-1}) from the carboxyl groups and the C–O–C stretching vibration (1159 cm^{-1}) from the epoxy groups.[23] After thermal treatment, the decreased intensities of the C=O and C–O–C stretching vibration of prGO demonstrated the partial reduction process.[24] Then, XRD was carried out to confirm the interlayer distance of the nanosheets (Fig. 1h) according to the Bragg equation. The dried GO sheets exhibited an intense peak at 10.3° with a *d*-spacing calculated to be 8.6 Å. Compared to the GO sheets, the prGO sheets showed a weakened peak at 11.7° corresponding to a *d*-spacing value of 7.6 Å. The decreased *d*-spacing and shifted peak position of prGO demonstrated the partial reduction of GO and the narrower *d*-spacing of prGO.[25] The Raman spectra (Fig. S2†) of GO and prGO showed the typical D peak (1347 cm^{-1}) and G peak (1592 cm^{-1}) for GO and a peak at 1587 cm^{-1} for prGO. The corresponding G peak of GO down-shifted from 1592 cm^{-1} to 1587 cm^{-1} after the thermal reduction. This resulted from the decrease in isolated double bonds resonating at a high frequency and the recovery of a hexagonal network of carbon atoms from prGO. The intensity ratio ID/IG of prGO (1.03) was lower than that of GO (1.05), which revealed that thermal reduction recovered the graphitic structure and reduced some defects.[26] XPS spectra were measured to determine the relative oxidation levels of GO and prGO. The C/O ratios of GO and prGO were 1.85 and 2.13 respectively, which proved there was a lower oxidation level for prGO. Thermal stability and degradation behaviors of the chemical bonds of GO and prGO were evaluated by TGA (Fig. S2†). GO and prGO foams were freeze-dried from aqueous dispersion and used as samples. First, the weight loss of GO (9.50%) and prGO (8.20%) over the temperature range of 25–150 °C was caused by water evaporation in the porous foams. The steep weight loss of GO and prGO between 150 and 235 °C corresponded to the release of CO$_2$ and H$_2$O from the decomposition of the labile groups. A small mass loss between 235 and 950 °C was attributed to the removal of more stable oxygen functionalities. The reduced water evaporation (8.20% for prGO and 9.50% for GO over the temperature range 25–150 °C) and larger residual weight of prGO (53.39% for prGO and 33.42% for GO) demonstrated the better thermostability of prGO, which was credited to fewer oxygen-containing groups.

Characterization of hybrid membranes based on prGO and CS

As shown in Scheme 1, the CS membrane was prepared by blade coating a CS dispersion onto a PS membrane and then was crosslinked by glutaraldehyde to form a Schiff base (R–C=N).[27] The prGO–CS membrane was fabricated by blade coating the prGO–CS composite on a PS membrane with embedded prGO sheets in a CS skin through the ring-opening reaction between the epoxy and amino groups.[14] Residual primary amine continued to be crosslinked by glutaraldehyde. The primary amine from CS (CS–NH$_2$) and secondary amine from prGO–CS (CS–NH–CH$_2$–CHOH–prGO) also participated in the protonation process, which endowed membranes with positive charges.

In order to characterize the surface and cross section morphology of the membranes, SEM images are presented.

Compared with the smooth morphology of the CS membrane (Fig. 2b and c), angular and wrinkled prGO nanosheets were observed in the prGO–CS membrane (Fig. 2d and e) because of the embedded architecture of the prGO nanosheets in CS. A free-standing prGO–CS membrane was fabricated to further reveal the embedded morphology of prGO in the CS layer on a large scale (Scheme 1 and Fig. 2f), which resulted from π–π self-stacking of the prGO sheets and the chemical reaction in the prGO–CS composite.[28]

AFM images (Fig. 3) are presented to characterize the surface roughness of the membranes. The CS membrane exhibited an ultra-smooth surface (R_q = 0.72 nm). The roughness of the prGO–CS membrane (R_q = 3.70 nm) was a little higher than the value for the CS membrane. The reason might be that the prGO
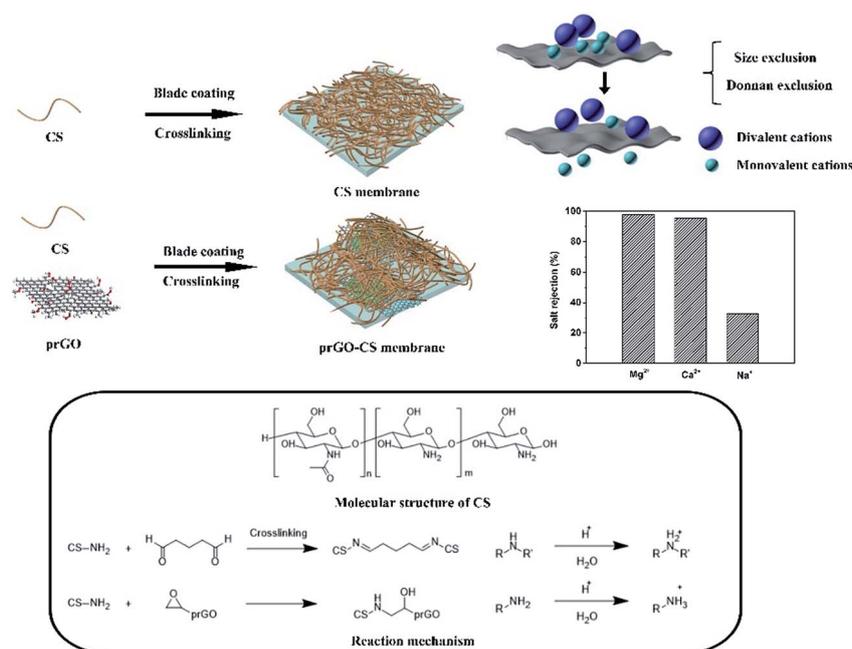
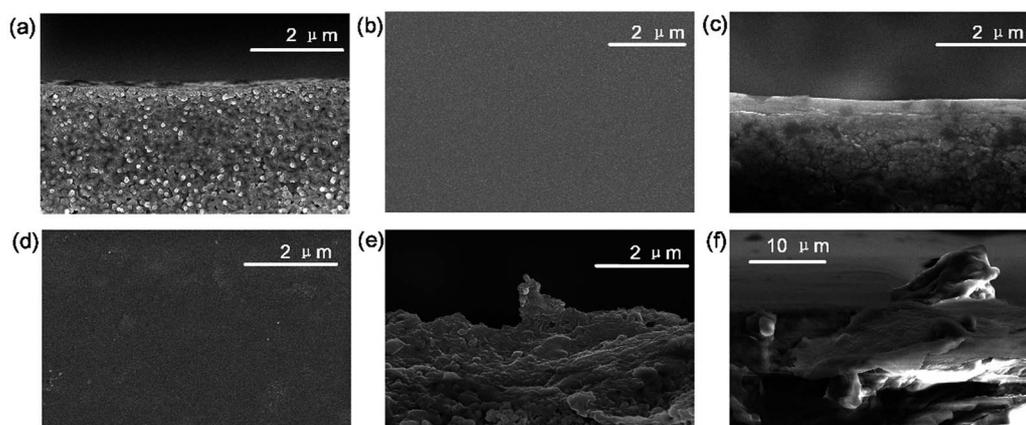Scheme 1 The reaction mechanism and preparation process of prGO and CS nanohybrid membranes.

Fig. 2 The SEM images of (a) the cross-section of PS, (b) the surface of CS, (c) the cross-section of CS, (d) the surface of prGO–CS, (e) the cross-section of prGO–CS, and (f) the cross-section of freestanding prGO–CS.
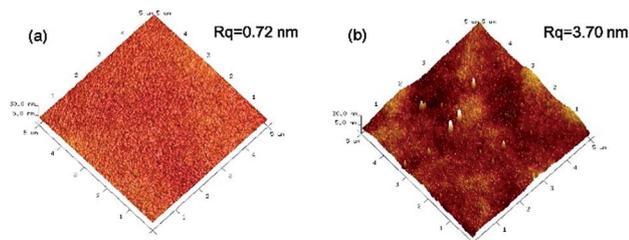
Fig. 3 The AFM images for (a) CS and (b) prGO–CS membranes.

sheets with sharp bulges were wrapped by CS molecules and then softened.

To characterize the wettability and surface properties of the membranes, photographs of the surface contact angle are presented (Fig. 4). After coating with CS, the surface contact angle of PS decreased from 74.5° to 23.0°, which resulted from the introduction of hydrophilic functional groups (amino, hydroxyl, *etc*). The surface contact angle of the prGO–CS membrane (25.7°) was slightly larger than that of the CS membrane (23.0°), revealing similar surface properties between CS and prGO–CS (Fig. 4b and c). These similar surface properties were supported by the similar water permeability between the CS and prGO–CS membranes (Fig. 6d).

Fig. 4 Photographs of water morphology on the (a) PS, (b) CS and (c) prGO–CS membrane surfaces.

XPS was used to analyze the elementary composition and verify the valence bond structure of the membranes by peak-differentiation-imitating analysis (Fig. S3† and Fig. 5a and b). The prGO–CS membrane had a lower amount of nitrogen than the CS membrane verifying the existence of N-free prGO nanosheets (Fig. S3†). Similarly, the prGO–CS membrane had a lower intensity of C–N and N–C=O than the CS membrane for the C 1s peak because of the introduction of prGO in CS (Fig. S3†). The prGO–CS membrane had a higher intensity of NH_2^+/NH_3^+ and C=N than the CS membrane for the N 1s peak (Fig. 5a and b). The increased intensity of NH_2^+/NH_3^+ and decreased intensity of NH/NH_2 were mainly caused by the ring-opening reaction in prGO–CS and the protonation of the amino groups.[29] The increased intensity of C=N showed the intensification of the cross-linking reaction by glutaraldehyde. Both of the ring-opening and cross-linking reactions gave the prGO–CS membrane a denser structure than the CS membrane, which was also demonstrated by the desalination performance outlined in the following text.

The FTIR-ATR spectra (Fig. 5c) were recorded to analyze the chemical structure of the CS and prGO–CS membranes. Free-standing CS and prGO–CS membranes were tested in order to eliminate the influence of the PS membrane. The FTIR characteristic peaks of CS and prGO–CS are the O–H stretching vibration (3261 cm^{-1}), the C–H stretching vibration (2901 cm^{-1}), the C=N stretching vibration (1630 cm^{-1}), the N–H stretching vibration (1530 cm^{-1}) and the C–O–C stretching vibration (1026 cm^{-1}).[30] The higher intensity of C=N in the crosslinked prGO–CS than that in the uncrosslinked one proved the formation of a Schiff base from the amino and aldehyde groups. The higher ratio of N–H to C=N in prGO–CS than that in CS indicated the occurrence of the ring-opening reaction.
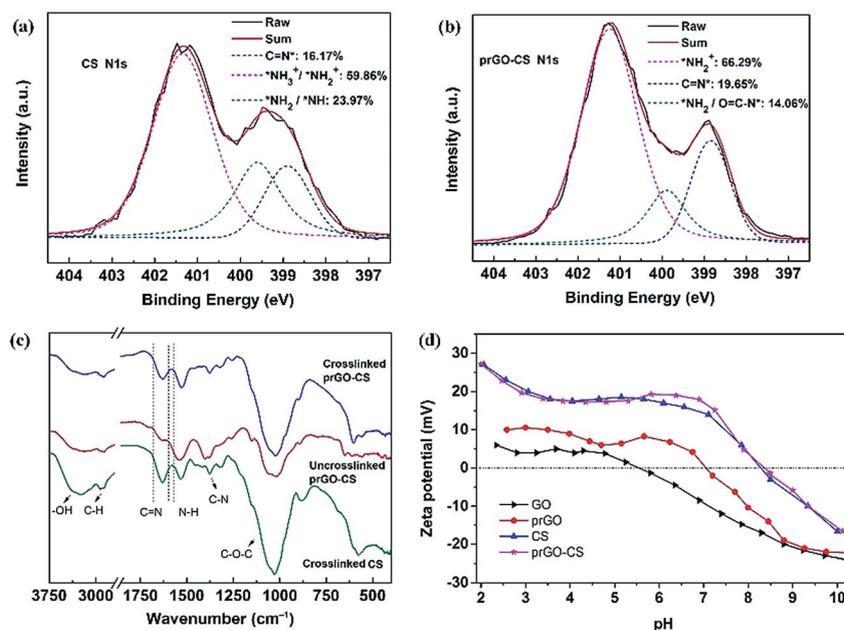

Fig. 5 The XPS survey spectra of N 1s for (a) CS and (b) prGO–CS membranes. (c) The FTIR-ATR spectra of CS and uncrosslinked and crosslinked prGO–CS. (d) The zeta potential of samples at different pH values.

The thermal stability and degradation behavior of the CS and prGO–CS free-standing membranes were evaluated by TGA (Fig. S4†). Similar decomposition temperatures of CS and prGO–CS were observed. A major weight loss between 200 °C and 340 °C was likely due to CS decomposition.[30] A slow weight loss between 340 °C and 900 °C was due to the partial decomposition of prGO. Compared with prGO–CS, CS showed a little more water evaporation over the temperature range of 25–150 °C, which could be ascribed to the stronger hydrophilicity of CS and is supported by the contact angle data (Fig. 4). This phenomenon also demonstrated the consumption of the hydrophilic groups (amino and hydroxyl groups) during the reaction between CS and prGO and the high chemical stability of the prGO–CS membrane.

The surface charges of the membranes were found to play an important role in salt rejection based on the well-known Donnan exclusion effect.[31] Therefore, the surface charge properties of the membranes in this work were studied by streaming zeta potential measurement (Fig. 5d). The surface charge was affected by the inherent charges, which resulted from protonation and dissociation of the surface functional groups. Due to the existence of oxygen-containing groups (–OH and –COOH), GO showed a negative charge over the pH range of 5.5–10. In contrast, prGO showed an isoelectric point (IEP) of pH 7.0 because of the thermal reduction of the oxygen-containing groups and the rebuilding of the carbon structure. The CS and prGO–CS membranes showed a positive charge over a pH range of 2–8.3, which covers the pH of brackish water with low salinity. Amino groups with lone pair electrons in CS could combine with a hydrogen ion and form positively charged ammonium. According to the Donnan exclusion effect, the positively charged CS and prGO–CS membranes (pH < 8.3) would result in a favorable electro-static repulsion to cations.[18]

Therefore, it is important to test the desalination performance of the nanohybrid membranes and explore the operating mechanism.

To evaluate the performance of the nanohybrid membranes, water flux and salt rejection of the membranes with different thicknesses of the CS layer and different assembly modes are shown in Fig. 6. As the thickness of the CS layer in wet conditions increased from 150 to 200 μm, salt rejection increased and water flux decreased rapidly (Fig. 6a and b). When the thickness changed from 200 to 250 μm, salt rejection increased slowly and water flux remained stable at around 20 L m^{-2} h^{-1} with a downward trend. Thus we studied the operating mechanism of different assembly methods on the premise that the thickness of the CS layer in wet conditions was 250 μm.

All membranes in this study followed a similar order for rejecting salts, i.e. $R(MgCl_2) > R(CaCl_2) > R(NaCl) > R(Na_2SO_4)$. On one hand, divalent cations (Mg^{2+} and Ca^{2+}) had a stronger electrostatic repulsion to the positively charged membrane than the monovalent anion (Na^+). The Donnan exclusion effect determined the order of rejected cations, i.e. $R(Mg^{2+}) > R(Ca^{2+}) > R(Na^+)$ and the order of rejected anions, i.e. $R(Cl^-) > R(SO_4^{2-})$. On the other hand, size exclusion determined the order of rejected cations. The hydrated ionic diameter of Mg^{2+}, Ca^{2+} and Na^+ is 8.56 Å, 8.24 Å and 7.16 Å.[32] Thus, the observed salt rejection order, i.e. $R(Mg^{2+}) > R(Ca^{2+}) > R(Na^+)$, was supported.

The desalination mechanism for the membranes in this work can be summed up as the synergy between size exclusion theory and Donnan exclusion theory.[31] For the rejection of Ca^{2+} and Mg^{2+}, the order was prGO–CS > CS (Fig. 6c). This proved that prGO played an important role in the increased rejection of divalent cations, which was due to the decreased d-spacing of prGO (7.6 Å) and increased compactness of the membrane by chemical bonding between prGO and CS (Fig. 5). In addition,
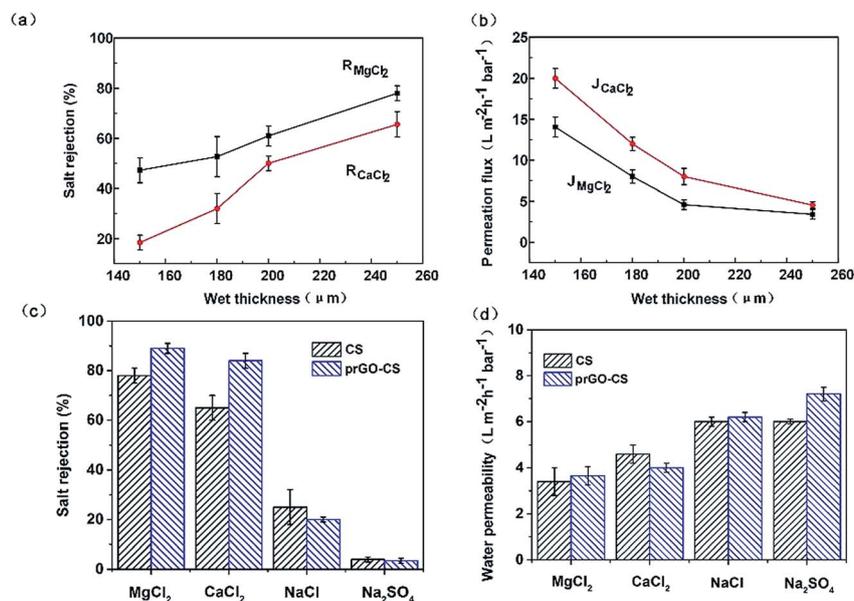

Fig. 6 The effect of thickness of the CS layer in a wet state on the (a) salt rejection and (b) permeation flux of the CS membrane (1 g L^{-1} MgCl$_2$ and CaCl$_2$ solution respectively, 25 °C, 5 bar). (c) The salt rejection and (d) permeation flux of membranes prepared by different methods for separating different salts (1 g L^{-1} MgCl$_2$, CaCl$_2$, NaCl and Na$_2$SO$_4$ solution respectively, 25 °C, 5 bar).

Table 1 Comparison of the performance of prGO–CS with several other flat-sheet membranes

Membrane	R_{MgCl_2} (%)	R_{CaCl_2} (%)	R_{NaCl} (%)	$R_{Na_2SO_4}$ (%)	J_{MgCl_2} (L m^{-2} h^{-1} bar^{-1})	J_{CaCl_2} (L m^{-2} h^{-1} bar^{-1})	Testing condition	$\alpha_{Mg^{2+}}^{Na^+}$	Ref.
prGO–CS	89.3	84.3	20.3	3.5	3.7	4.0	1 g L^{-1}, 5 bar	7.4	This work
CS	87.7 (Mg_2SO_4)	—	27.8	—	—	—	2 g L^{-1}, 4.8 bar	5.9	33
PSDA	66.1	65.8	37.2	20.1	6.0	6.0	1 g L^{-1}, 5 bar	1.9	34
PEC-NFM-5	94.0	—	37.9	6.2	2.2	—	1 g L^{-1}, 6 bar	10.4	35
DA/PEIc	89.3	—	27.3	—	5.5	—	1 g L^{-1}, 8 bar	6.8	36
PAN/PEIc	92.8	—	61.3	—	1.6	—	2 g L^{-1}, 10 bar	5.4	36
HACC	83.1	—	13.7	12.5	3.6	—	1 g L^{-1}, 3 bar	5.1	37

prGO–CS showed a higher zeta potential than the CS membrane over a pH range of 6–8.3 and had a stronger electrostatic repulsion to divalent cations. It is worth mentioning that the water fluxes of the prGO–CS membrane (about 20 L m^{-2} h^{-1}) were not lower than those of the CS membrane, though they showed a nice performance boost in the removal of Ca^{2+} and Mg^{2+}. This was probably due to the similar surface properties (Fig. 3 and 4) and water channels created in the prGO–CS composite.

The prGO–CS membrane showed nearly 90% rejection of MgCl$_2$ and nearly 85% rejection of CaCl$_2$ under a low pressure of 5 bar. The salt rejection of the membranes was less than 20% for NaCl and less than 10% for Na$_2$SO$_4$. The comparison of the performance of prGO–CS with several other flat-sheet positively charged membranes is shown in Table 1.[33–37] prGO–CS exhibited excellent performance in terms of Na$^+$/Mg^{2+} selectivity. This indicates that the prGO and CS nanohybrid membranes show great potential for the separation of univalent and divalent cations.

The prGO–CS membrane in this work showed a decreased rejection of divalent cations (70% rejection for MgCl$_2$ and CaCl$_2$) using high-concentration solutions (0.1 mol L^{-1}). This phenomenon was due to the weakened Donnan exclusion effect. The degree of compactness of the membrane is the determining factor that affects rejection performance based on the synergistic mechanism. The method of increasing the crosslinking reaction time was tried to further explore the desalination mechanism. The prGO–CS membrane with the longer crosslinking reaction time showed a high rejection of divalent cations (90% rejection for MgCl$_2$ and 85% rejection for CaCl$_2$) when using high-concentration solutions (0.1 mol L^{-1}), although the flux decreased (less than 1 L m^{-2} h^{-1} bar^{-1}). The experimental results demonstrated that there is synergy between the size exclusion theory and Donnan exclusion theory for prGO–CS membranes.

In order to simulate practical application in brackish water, we designed a cross-flow filtration experiment in 3000 ppm TDS mixed salt feed solution.[38] As shown in Table 2, the prGO–CS membrane showed a rejection of 98.0% towards MgCl$_2$, rejection of 95.5% towards CaCl$_2$ and a high Na$^+$/Mg^{2+} selectivity of 33.8, which demonstrated its promise in brackish water softening. This is attributed to the dense structure, controllable positive charge and water channels in the prGO and CS nanohybrid membranes.

Conclusions

In summary, a facile method of configuration adjustment and surface charge control was developed to fabricate prGO and CS nanohybrid membranes to block divalent cations and allow monovalent cations through. prGO sheets were synthesized to deliver both reduced *d*-spacing and good solution processability. The prGO–CS membranes with a CS skin and embedded prGO sheets showed a desalination performance improvement of nearly 98.0% rejection of MgCl$_2$ and nearly 95.5% rejection of CaCl$_2$, which was attributed to the dense structure and positive charge of prGO–CS. The high Na$^+$/Mg^{2+} selectivity of the prGO–CS membrane demonstrates a great prospect for brackish water softening and shows potential applications in classification and concentration, such as descaling for circulation cooling water systems, demineralizing and concentrating for whey protein and the removal of BOD/COD for devices under low system pressure.

Conflicts of interest

There are no conflicts to declare.

Table 2 Performance of prGO–CS for feed solution with various ion compositions (TDS = 3000 ppm, 10 bar, Mg^{2+} = 128 ppm, Ca^{2+} = 325 ppm, Na$^+$ = 631 ppm)

Membrane	Rejection (%)			J (L m^{-2} h^{-1} bar^{-1})	$\alpha_{Mg^{2+}}^{Na^+}$	$\alpha_{Ca^{2+}}^{Na^+}$
	Mg^{2+}	Ca^{2+}	Na$^+$			
prGO–CS	98.0	95.5	32.5%	1.5	33.8	15.0

Notes and references

1 P. Sun, K. Wang and H. Zhu, *Adv. Mater.*, 2016, **28**, 2287–2310.

2 R. K. Joshi, P. Carbone, F. C. Wang, V. G. Kravets, Y. Su, I. V. Grigorieva, H. A. Wu, A. K. Geim and R. R. Nair, *Science*, 2014, **343**, 752–754.

3 L. Huang, M. Zhang, C. Li and G. Shi, *J. Phys. Chem. Lett.*, 2015, **6**, 2806–2815.

4 G. Liu, W. Jin and N. Xu, *Chem. Soc. Rev.*, 2015, **44**, 5016–5030.

5 S. Zheng, Q. Tu, J. J. Urban, S. Li and B. Mi, *ACS Nano*, 2017, **11**, 6440–6450.

6 Y. H. Xi, Z. Liu, J. Ji, Y. Wang, Y. Faraj, Y. Zhu, R. Xie, X. J. Ju, W. Wang, X. H. Lu and L. Y. Chu, *J. Membr. Sci.*, 2018, **550**, 208–218.

7 L. Qiu, X. Zhang, W. Yang, Y. Wang, G. P. Simon and D. Li, *Chem. Commun.*, 2011, **47**, 5810.

8 Y. Han, Z. Xu and C. Gao, *Adv. Funct. Mater.*, 2013, **23**, 3693–3700.

9 B. Mi, *Science*, 2014, **343**, 740–742.

10 X. Xu, F. Lin, Y. Du, X. Zhang, J. Wu and Z. Xu, *ACS Appl. Mater. Interfaces*, 2016, **20**, 12588–12593.

11 J. Abraham, K. S. Vasu, C. D. Williams, K. Gopinadhan, Y. Su, C. T. Cherian, J. Dix, E. Prestat, S. J. Haigh, I. V. Grigorieva, P. Carbone, A. K. Geim and R. R. Nair, *Nat. Nanotechnol.*, 2017, **12**, 546–550.

12 Q. Nan, P. Li and B. Cao, *Appl. Surf. Sci.*, 2016, **387**, 521–528.

13 X. Song, R. S. Zambare, S. Qi, B. N. Sowrirajalu, A. P. James Selvaraj, C. Y. Tang and C. Gao, *ACS Appl. Mater. Interfaces*, 2017, **47**, 41482–41495.

14 L. Shao, X. Chang, Y. Zhang, Y. Huang, Y. Yao and Z. Guo, *Appl. Surf. Sci.*, 2013, **280**, 989–992.

15 S. P. Dharupaneedi, R. V. Anjanapura, J. M. Han and T. M. Aminabhavi, *Ind. Eng. Chem. Res.*, 2014, **53**, 14474–14484.

16 A. Shirdast, A. Sharif and M. Abdollahi, *J. Power Sources*, 2016, **306**, 541–551.

17 S. Sayyar, E. Murray, S. Gambhir, G. Spinks, G. G. Wallace and D. L. Officer, *J. Occup. Med.*, 2016, **68**, 384–390.

18 J. Wang, X. Gao, J. Wang, Y. Wei, Z. Li and C. Gao, *ACS Appl. Mater. Interfaces*, 2015, **7**, 4381–4389.

19 H. M. Hegab, Y. Wimalasiri, M. Ginic-Markovic and L. Zou, *Desalination*, 2015, **365**, 99–107.

20 Z. Xu, H. Sun, X. Zhao and C. Gao, *Adv. Mater.*, 2013, **25**, 188–193.

21 W.-S. Hung, Q.-F. An, M. De Guzman, H.-Y. Lin, S.-H. Huang, W.-R. Liu, C.-C. Hu, K.-R. Lee and J.-Y. Lai, *Carbon*, 2014, **68**, 670–677.

22 L. Ouyang, R. Malaisamy and M. L. Bruening, *J. Membr. Sci.*, 2008, **310**, 76–84.

23 D. C. Marcano, D. V. Kosynkin, J. M. Berlin, A. Sinitskii, Z. Sun, A. Slesarev, L. B. Alemany, W. Lu and J. M. Tour, *ACS Nano*, 2010, **4**, 4806–4814.

24 H. Zhao, S. Chen, X. Quan, H. Yu and H. Zhao, *Appl. Catal., B*, 2016, **194**, 134–140.

25 Q. Zheng, W. H. Ip, X. Lin, N. Yousefi, K. K. Yeung, Z. Li and J.-K. Kim, *ACS Nano*, 2011, **5**, 6039–6051.

26 L. Zou, *J. Membr. Sci.*, 2016, **515**, 204–211.

27 D. A. Musale and A. Kumar, *Sep. Purif. Technol.*, 2000, **21**, 27–37.

28 C.-H. Tsou, Q.-F. An, S.-C. Lo, M. De Guzman, W.-S. Hung, C.-C. Hu, K.-R. Lee and J.-Y. Lai, *J. Membr. Sci.*, 2015, **477**, 93–100.

29 T. Sugama and M. Cook, *Prog. Org. Coat.*, 2000, **38**, 79–87.

30 S. Sayyar, E. Murray, S. Gambhir, G. Spinks, G. G. Wallace and D. L. Officer, *J. Occup. Med.*, 2016, **68**, 384–390.

31 N. Hilal, H. Al-Zoubi, N. A. Darwish, A. W. Mohamma and M. Abu Arabi, *Desalination*, 2004, **170**, 281–308.

32 E. R. Nightingale Jr, *J. Phys. Chem.*, 1959, **63**, 1381–1387.

33 D. A. Musale and A. Kumar, *J. Appl. Polym. Sci.*, 2000, **77**, 1782–1793.

34 Z. Zhao, A. Wu, S. Luan and C. Zhang, *J. Polym. Res.*, 2015, **22**, 168.

35 F.-Y. Zhao, Q.-F. An, Y.-L. Ji and C.-J. Gao, *J. Membr. Sci.*, 2015, **492**, 412–421.

36 M. Li, J. Xu, C. Y. Chang, C. Feng, L. Zhang, Y. Tang and C. Gao, *J. Membr. Sci.*, 2014, **459**, 62–71.

37 R. Han, J. Zeng, Y. Wang, Q. Chang, X. Zhang and J. Zhou, *Desalin. Water Treat.*, 2014, **52**, 5790–5795.

38 W. Fang, L. Shi and R. Wang, *J. Membr. Sci.*, 2013, **430**, 129–139.